Chain Folding in Liquid-Crystalline Main-Chain Polymers with a Smectic Phase

Armelle Vix,[†] Wolfgang Stocker,*[,†] Manfred Stamm,[‡] Götz Wilbert,[§] Rudolf Zentel,[§,||] and Jürgen P. Rabe[†]

Department of Physics, Humboldt University Berlin, Invalidenstrasse 110, D-10115 Berlin, Germany, Max-Planck-Institute for Polymer Research, Ackermannweg 10, Postfach 3148, D-55021 Mainz, Germany, and Institute for Organic Chemistry, Johannes Gutenberg University, J.-J.-Becher Weg 18-20, D-55099 Mainz, Germany

Received May 12, 1998; Revised Manuscript Received October 16, 1998

ABSTRACT: Thermotropic main-chain liquid-crystalline polymers (LCPs) composed of azobenzene or azoxybenzene mesogens and flexible spacers with and without a phenyl side group have been characterized by gel permeation chromatography, differential scanning calorimetry, and X-ray diffraction. The polymers exhibit smectic phases in the well-accessible temperature range from room temperature up to 160 °C. The morphology of thin films on a solid substrate was studied by X-ray reflectometry and scanning force microscopy (SFM). The smectic layers are mainly oriented parallel to the film surface. On the basis of X-ray reflectometry and SFM investigations, it is concluded that, at least in thin films, the polymer main chains are not extended like in the common model for main-chain LCPs, but almost regularly folded.

Introduction

Many main-chain liquid-crystalline polymers (LCPs) have been synthesized and investigated for more than 10 years.[1,2] In main-chain LCPs, the mesogenic groups within the polymer backbone are linked to each other through a flexible spacer. Each mesogenic group participates in forming the mesophase structure, but the polymer chains must adopt a conformation or packing that is compatible with the structure of the mesophase. This important structural aspect of polymer-chain conformation has been extensively studied both theoretically[3,4] and experimentally.[5−9] de Gennes first pointed out that a semiflexible long chain in the nematic phase may recover some part of the entropy lost because of the ordering of the mesogenic units by forming "hairpin" foldings where the chain executes a counter-reversal (180°) with respect to the director.[3] Statics and dynamics of hairpins in nematic liquid crystals have been studied theoretically by Williams et al.[4] The formation of hairpins has been confirmed experimentally by X-ray diffraction experiments[5−8] and neutron scattering.[9,10] The existence of hairpins was established in both nematic[9,10] and smectic[7] main-chain LCPs.

In the present paper, three smectic main-chain LCPs, named P1, P2, and P4, are analyzed. Synthesis has been described elsewhere.[11−14] The studies have several objectives: (a) The first is to characterize the samples in order to analyze their molecular weights from gel permeation chromatography (GPC), phase transitions from differential scanning calorimetry (DSC), and layer spacings from X-ray scattering. (b) The second is the analysis of the orientation of smectic layers in thin films by X-ray reflectometry and scanning force microscopy (SFM). (c) The third is, as indicated above, to confirm the hairpin formation in thin films of smectic main-chain LCPs.

* To whom correspondence should be addressed.
[†] Humboldt University Berlin.
[‡] Max-Planck-Institute for Polymer Research.
[§] Johannes Gutenberg University.
[||] Present address: Institute for Material Science, Faculty of Chemistry, BU/GH Wuppertal, Gauss Strasse 20, D-42097 Wuppertal, Germany.

Experimental Section

Synthesis and Characterization. Three main-chain polymers, P1, P2, and P4 (Table 1), have been investigated. They are polyesters with azoxybenzene (P1, P2) or azobenzene (P4) units as mesogens, separated by flexible spacers. Polymers P2 and P4 have a phenyl side group linked laterally to the main-chain spacer. The synthesis of the mesogenic groups 4,4′-bis-[(6-hydroxyhexyl)oxy]azoxybenzene (in P1 and P2) and 4,4′-bis[(6-hydroxyhexyl)oxy]azobenzene (in P4) is described elsewhere.[11−14] The comonomers diethyl malonate and diethyl phenylmalonate were purchased from Aldrich. The polymers were synthesized via melt polycondensation catalyzed with 2−3 drops of $Ti(O\text{-}iPr)_4$. The monomers were placed in a Schlenk flask in equimolar amounts and heated to 140 °C in a stream of dry nitrogen. Then the catalyst was added, and the procedure was carried out according to ref 13. The molecular weights of the polymers were determined by GPC in chloroform calibrated against polystyrene standards. The thermotropic behavior was studied by differential scanning calorimetry (DSC30, Mettler Toledo, rate 10 °C/min) and by polarization microscopy (Zeiss-Jenapol apparatus with an integrated THM 600 hotstage, Linkam Industry). For an accurate identification of the LC phases and for the elucidation of the molecular packing, X-ray investigations were performed on both unoriented and oriented samples. Unoriented samples were prepared by depositing a small quantity of the material on a holder, which was then slightly heated (up to 50−70 °C) to favor the formation of a compact bulk. These unoriented samples were investigated at room temperature with a flat-plate camera using Cu Kα radiation ($\lambda = 1.54$ Å). Temperature-dependent X-ray measurements were performed with a $\theta-\theta$ goniometer (D500 diffractometer, Siemens) under vacuum. Because of the slit geometry in the temperature-dependent experiments, one has to consider slit smearing effects at small scattering angles. It turns out that smearing has only a significant effect on peak positions when large spacings are considered ($d > 5$ nm). The small corrections in the case of our samples are well within the errors of the values given.

The oriented fibers were prepared by pulling up the highly viscous isotropic melt with tweezers and succeedingly elongat-

10.1021/ma9807567 CCC: $15.00
Published on Web 12/03/1998

Table 1

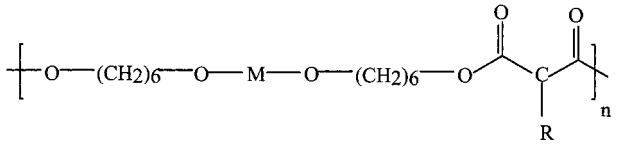

Polymer	Mesogen M	Side group R
P1	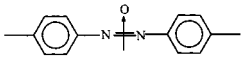	
P2	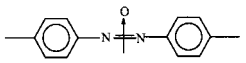	
P4	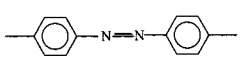	

ing it with a speed of approximately 1 m/s. The fibers were analyzed by X-ray measurements with a flat-plate camera at room temperature.

Film Preparation. For X-ray reflection and SFM, thin films of P1, P2, and P4 were prepared on silicon substrates. The films were prepared by spin-coating the polymers from a 10 mg/mL solution in a 50/50 (v/v) solvent mixture of dichloromethane and chloroform. A total of 2−3 mL of the solvent was dropped on the rotating silicon substrate. The rotation speed of the silicon substrate was about 2000 rpm. The films which were analyzed in the present study show a thickness in the range between 5 and 15 nm. Decreasing the concentration results in thinner films. The film thickness has been determined by X-ray reflectometry experiments before and after annealing above 100 °C.

X-ray Reflectometry. X-ray reflectometry experiments were carried out using a conventional X-ray reflectometer[15] with a copper target. A pyrolytic graphite monochromator is used in front of the scintillation counter. Collimation of the beam by slits leads to a beam divergence of 0.01°. The measurement at 100 °C was done in a heatable vacuum cell. The temperature of the polymer film was measured directly on the surface. During the measurement, the temperature was kept constant to ±0.1 °C. To equilibrate the sample, the measurement was started after 45 min of annealing time.

SFM. SFM measurements were performed with a commercially available Nanoscope IIIa (Digital Instrument Inc., Santa Barbara, CA). Image acquisition was performed at the air−polymer interface in the tapping mode. In this mode the cantilever is oscillating vertically at its resonance frequency, touching the sample surface periodically. Therefore, lateral shear forces are minimized and accordingly also tip-induced sample degradation. Silicon cantilevers (length 125 μm, width 30 μm, thickness 3−5 μm) with a spring constant between 17 and 64 N/m and a resonance frequency in the range of 240−400 kHz were used. Scratching a gap in the films with a needle reveals the substrate and makes it possible to determine the film thicknesses by SFM.

Molecular Modeling. Molecular modeling was performed on a Silicon Graphics computer system using the molecular modeling package Discover Version 4.0, Biosym Technologies Inc., San Diego, CA.

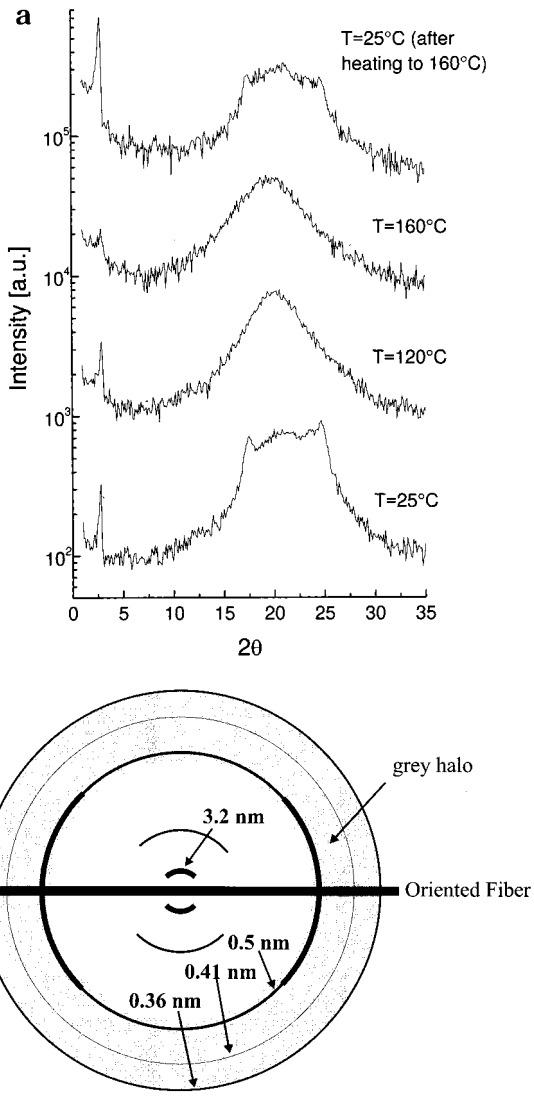

Figure 1. (a) X-ray diffraction patterns recorded from unoriented samples of polymer P1 at different temperatures. For clarity the curves are shifted against each other by 1 order of magnitude. (b) Schematic representation of the small- and wide- angle X-ray diffraction patterns recorded on oriented fibers of polymer P1. The fiber axis is drawn schematically in the figure. The patterns indicate the orientation of smectic layers predominantly parallel to the fiber axis.

Results

Characterization of the LC Polymers. The molecular weights of the polymers as determined by GPC are summarized in Table 2, revealing molecular weights in the range of 8.5×10^3−28.5×10^3 g/mol. All unoriented polymers exhibit birefringence in the polarization microscope, but no well-known LC texture was

Table 2

polymer	mol wt (10^3 g/mol)	phase transitions[a] (°C)	smectic layer spacing (nm) XRD[b]	XRD[c]	SFM[d]
P1	$M_W = 28.5$ ($M_W/M_N = 2.9$)	g 16 s_x 109 s_A 159 i	3.26 ± 0.05	3.2 ± 0.1	3.6 ± 0.3
P2	$M_W = 15.6$ ($M_W/M_N = 2.4$)	g 23 s_A 123 i	3.53 ± 0.06	3.7 ± 0.1	3.8 ± 0.3
P4	$M_{max} = 8.56$[e]	g 29 s_B 54 s_A 117 i	3.5 ± 0.1	3.8 ± 0.1	3.6 ± 0.3

[a] g = glass, s = smectic, and i = isotropic. [b] As determined from X-ray powder diffraction at room temperature. [c] As determined from the X-ray diffraction on oriented fibers. [d] Outermost smectic layer thickness as obtained from the SFM cross-sectional profile. [e] Peak maximum obtained from the GPC elution diagram.

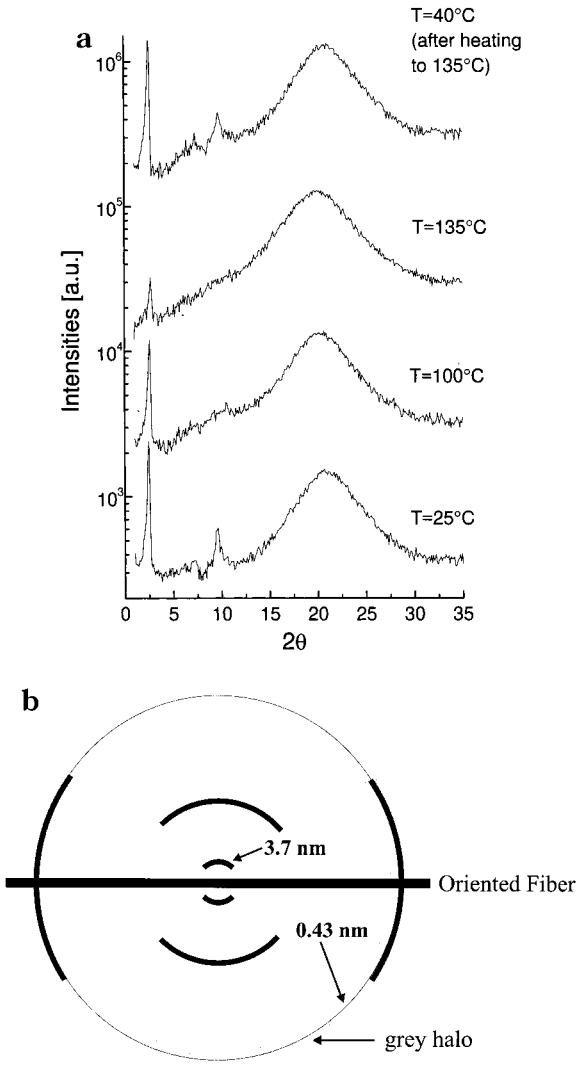

Figure 2. (a) X-ray diffraction patterns recorded from unoriented samples of polymer P2 at different temperatures. For clarity, the curves are shifted against each other by 1 order of magnitude. (b) Schematic representation of the small- and wide-angle X-ray diffraction patterns recorded from oriented fibers of polymer P2. The patterns were obtained at room temperature for a long accumulating time per angle. The patterns indicate the orientation of smectic layers predominantly parallel to the fiber axis.

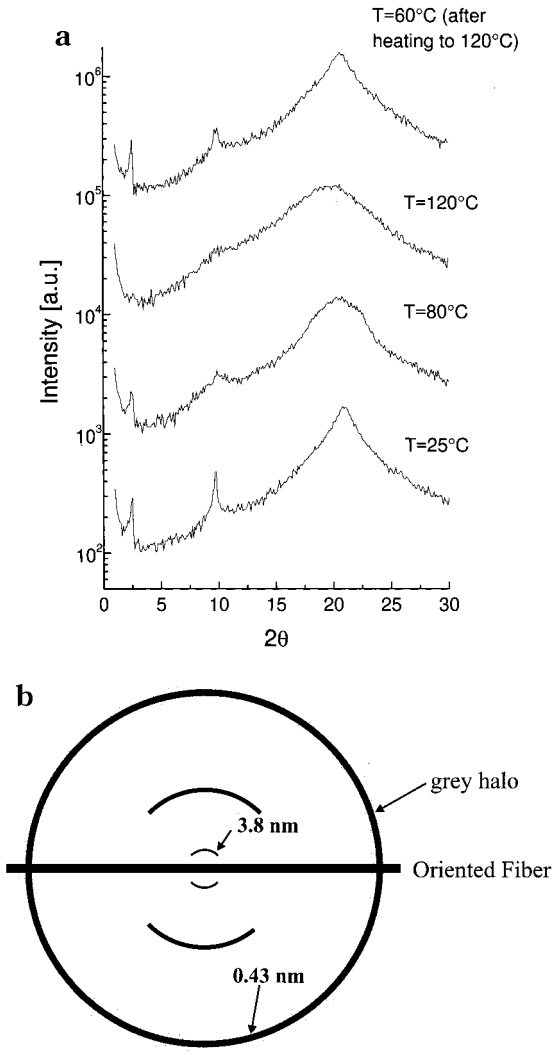

Figure 3. (a) X-ray diffraction patterns recorded from unoriented samples of the polymer P4 at different temperatures. For clarity, the curves are shifted against each other by 1 order of magnitude. (b) Schematic representation of the small- and wide-angle X-ray diffraction pattern obtained from oriented fibers of P4. The small-angle spots indicate the orientation of smectic layers predominantly parallel to the fiber axis.

recognizable. Nevertheless, mesophases could be assigned by means of phase transition temperatures resulting from DSC and X-ray diffraction measurements as elucidated below. Synthesis and DSC thermograms are published elsewhere.[12−14]

X-ray diffraction results for an unoriented sample of polymer P1 obtained at different temperatures are displayed in Figure 1a. At 25 °C, the diffraction curve exhibits a sharp small-angle peak at $2\theta = 2.7° \pm 0.2°$, which corresponds to a periodic distance of $d = 3.27 \pm 0.05$ nm. Spacings as determined from small-angle X-ray diffraction peaks are summarized in Table 2. In the wide-angle range, a halo appears between $2\theta = 15°$ and 27°, composed of some poorly resolved peaks. This halo is completely smeared out when the sample is heated above 60 °C, indicating a phase transition into a smectic phase. The intensity of the small-angle peak decreases with increasing temperature and disappears above 160 °C, and it reappears upon cooling (Figure 1a). For an oriented fiber of P1, small- and wide-angle X-ray diffraction patterns were obtained with the flat-plate camera. The results are schematically shown in Figure 1b. Broad reflection maxima (arcs) with a spacing of 3.2 ± 0.1 nm and their extremely weak fourth order can be seen on the meridian. Additionally, a broad outer reflection with a spacing of around 0.5 nm can be seen on the equator. Moreover, the X-ray diffraction pattern shows the wide-angle diffuse halo in the range of $15° < 2\theta < 24°$ with a weak ring at $2\theta = 21.6° \pm 0.2°$ (0.41 ± 0.05 nm) and a more intense ring at $2\theta = 24.6° \pm 0.2°$ (0.36 ± 0.05 nm), classically due to the lateral interferences between mesogenic cores. The composite small- and wide-angle patterns indicate that the smectic layers are oriented predominantly parallel to the fiber axis.

Similar investigations were performed for polymer P2. For the unoriented sample, like in the case of P1, a sharp small-angle peak is found at $2\theta = 2.5° \pm 0.1°$ (3.53 ± 0.06 nm) for a temperature range of 25−135 °C (Figure 2a). The spacing is slightly increased which respect to P1, indicating that the presence of the phenyl side group affects the layer spacing. An amorphous halo occurs at $14° < 2\theta < 28°$ without any structure already at room temperature. With increasing temperature, the intensity of the small-angle peak decreases. Unlike for

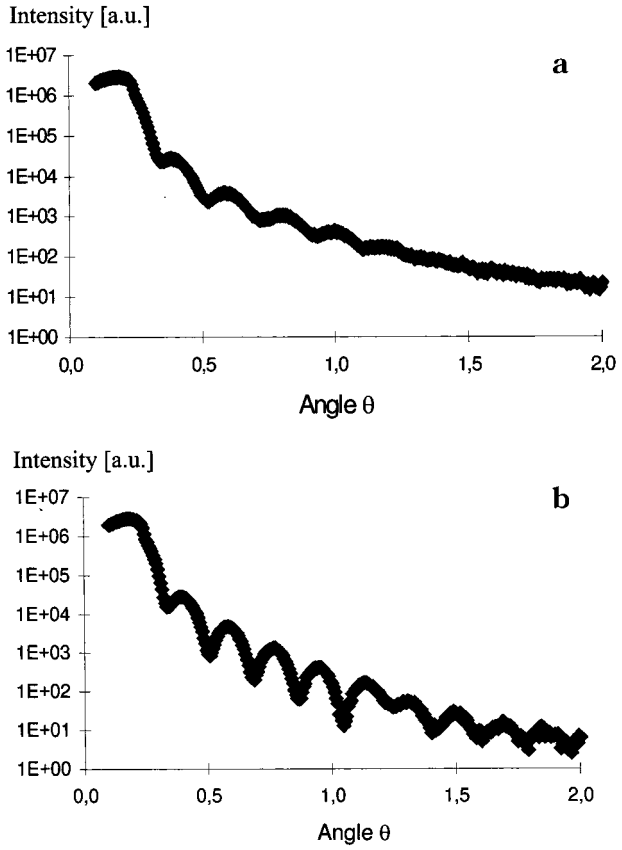

Figure 4. X-ray reflectivity pattern recorded from a 12.5 nm thick film of sample P2 obtained at (a) 100 °C and (b) room temperature. After cooling of the sample to room temperature (b), the Kiessig fringes are much more pronounced and the influence of a Bragg reflection of 3.4-nm spacing is clearly evident.

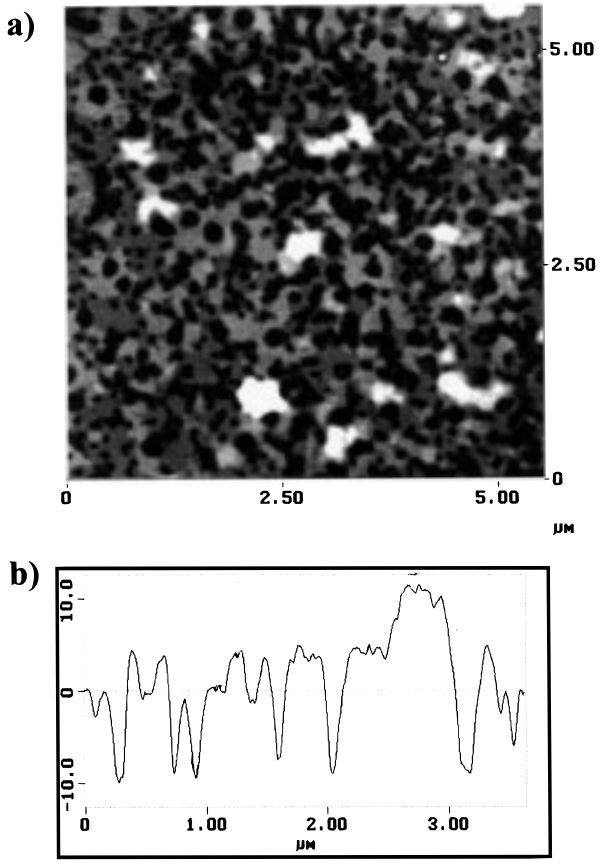

Figure 5. Formation of a smectic island network on top of a film of P1. SFM image (5 × 5 μm) of an oriented film at the polymer−air interface (black−white contrast: 25 nm). Horizontal cross section of the image shown above. The height difference between the smectic layers is 3.3 ± 0.5 nm.

P1, however, at room temperature a well-defined fourth-order Bragg peak occurs for $2\theta = 9.6° \pm 0.2°$. At higher temperatures, the intensity of this peak weakens, and it vanishes above 60°. Upon cooling, both peaks reappear in the same temperature range. The fiber pattern of P2 at room temperature (Figure 2b) reveals the presence of a layer spacing of 3.7 ± 0.1 nm (inner reflections) and predominantly orthogonal arcs with respect to the layer spacing, corresponding to 0.43 ± 0.05 nm. A diffuse halo occurs in the range between 2θ = 17° and 25°. These broad outer reflections are attributed to the distance between the neighboring mesogens within a layer. In analogy to P1, it can be concluded that the smectic layers are oriented predominantly parallel to the fiber axis.

For polymer P4, small-angle Bragg peaks were also observed up to the fourth order. For temperatures up to 120 °C (Figure 3a), the first-order Bragg peak occurs at $2\theta = 2.5° \pm 0.2°$, corresponding to a spacing of d = 3.5 ± 0.1 nm. Like polymer P2, the disappearance of both Bragg peaks is reversible upon raising of the temperature. Additionally, a relatively pronounced halo is observed in the wide-angle region, corresponding to an average spacing of about 0.4 nm. This halo is getting broader upon heating of the sample. Above 120 °C, the low-angle reflection disappears, indicating the phase transition into the isotropic state. The fiber pattern at room temperature (Figure 3b) reveals the presence of a layer spacing of 3.8 ± 0.1 nm (inner reflections on the meridian). The inner reflections suggest that the smectic layers are oriented mainly parallel to the fiber axis. In the wide-angle range, an amorphous halo occurs, centered at 0.4 ± 0.1 nm.

Analysis of Thin Films. To determine the total film thickness and the orientation of smectic layers within the film, X-ray reflection experiments were carried out on thin films of polymer P2. Figure 4 shows the results at 100 °C (a) and after cooling to room temperature (b). At high temperatures (Figure 4a), one can first recognize damped Kiessig fringes which are due to interferences resulting from both interfaces. The total film thickness of about 12.5 nm is determined from the angular spacing of these intensity maxima. The damping is caused by the surface roughness, which should be on the order of 2−4 nm (root mean square). The material is in an isotropic state, and a Bragg reflection cannot be identified. After cooling of the sample to room temperature (Figure 4b), the Kiessig fringes are much more pronounced and the influence of a Bragg reflection of 3.4-nm spacing becomes clearly evident. Therefore, one can conclude that the surface roughness is much smaller (on the order of 1 nm) and that smectic layers are ordered parallel to the surface. The Bragg peak of the layer spacing is not very pronounced because of the limited film thickness so that only four smectic layers can contribute to the peak. Therefore, it is quite broad and low in intensity, while it is coherently superimposed with the Kiessig fringes. This gives rise to the observed change in the modulation. The effect would hardly be detectable if there would be no orientation of the layers parallel to the surface. Similar results were obtained on P1 and P4.

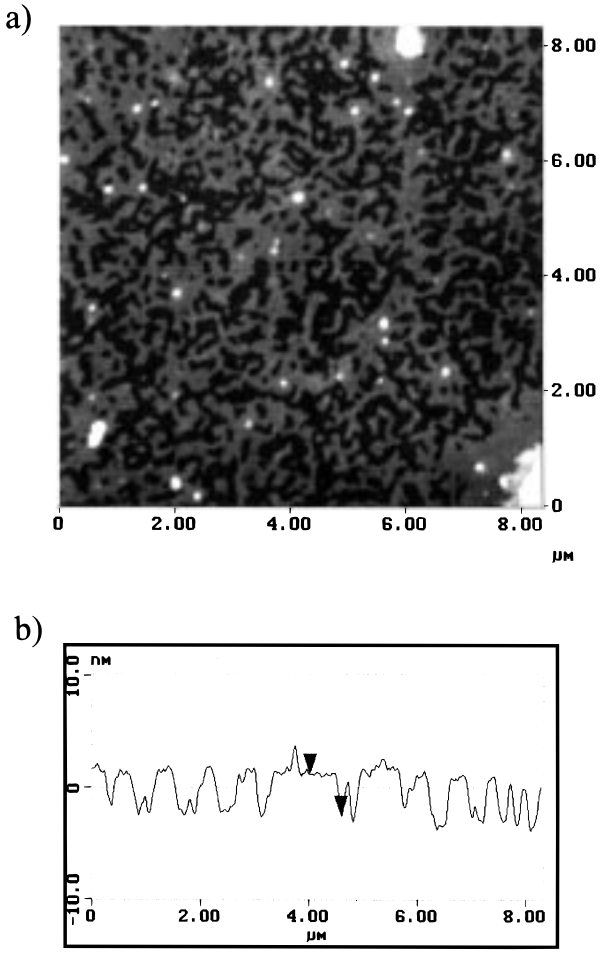

Figure 6. Formation of a smectic island network on top of a thin film of P2. SFM image (8 × 8 μm) of an oriented film at the polymer−air interface (black−white contrast: 20 nm). Horizontal cross section of the image shown above. The height difference between two smectic layers is 3.5 ± 0.5 nm.

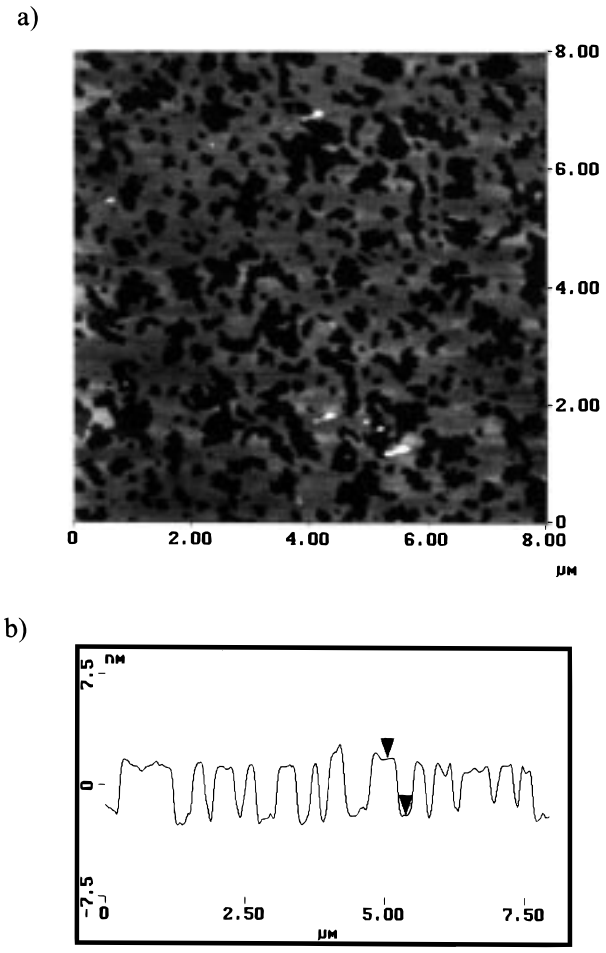

Figure 7. Formation of a smectic island network on top of a thin film of P4. SFM image (8 × 8 μm) of an oriented film at the polymer−air interface (black−white contrast: 20 nm). Horizontal cross section of the image shown above. The height difference between two smectic layers is 3.5 ± 0.5 nm.

SFM analyses were performed on spin-coated films after annealing of the films for several days above T_g. The film thicknesses were about 8, 10, and 7 nm for P1, P2, and P4, respectively. SFM images are displayed in Figures 5a, 6a, and 7a. It should be mentioned that Figures 5−7 not only display particularly well-ordered regions but also show the characteristic structure of the films which can be found in any places of the sample. The three LC polymers show the presence of islands at the surface of the film similar to the case of combined and side-chain LCPs investigated earlier.[16,17] The surfaces reveal two well-defined heights as evidenced by the cross-sectional profiles (Figure 5b, 6b, and 7b) along lines of the height scans. The vertical heights of these islands are 3.6 ± 0.3, 3.8 ± 0.3, and 3.6 ± 0.3 nm for P1, P2, and P4, respectively. These values compare well to a smectic layer in the polymer bulk. However, because of the uncertainty in the determination of the heights of these islands by SFM, the values do not allow one to distinguish the small differences in spacing for the three polymers as is possible by X-ray diffraction (Table 2).

Discussion

The results presented above show that all studied polymers are able to order in a smectic phase. The question arises then, how do they pack in this phase? The polymer chains must adopt a conformation or packing that is compatible with the structure of the mesophase. We have estimated the average thickness of a smectic layer in two different conformations using a molecular modeling package (Discover Version 4.0, Biosym Technologies Inc., San Diego, CA). We consider two models for describing the smectic mesophase: in model A, the polymer chains are mainly extended, only occasionally forming hairpin loops (Figure 8a); in model B, the polymer chains are almost regularly folded (Figure 8b). In the latter model, the flexible spacer is bent in the region between the mesogen and the phenyl side group so that the phenyl ring is oriented away from the hairpin and parallel to the chain orientation. The stiff mesogens may be shifted relative to each other like it is in the case of the crystalline phase of the corresponding low molecular weight azobenzene[18] or azoxybenzene mesogen.[19] To differentiate between models A and B, one may compare the length of one repeat unit of the polymer and the thickness of the smectic layers. If the polymer backbone is considered mainly extended, the thickness of the smectic layers should not exceed the length of a completely stretched repeat unit (Figure 8a). Depending on whether the polymer backbone is in a stretched conformation or whether it has a bent flexible spacer, we determined its length from the molecular modeling to be either 3.3 or 3.8 nm. Without the phenyl side group as is the case for P1, a spacing of 3.3 nm is expected for both models (Figure 8). The values have an error margin of about 5%. These values

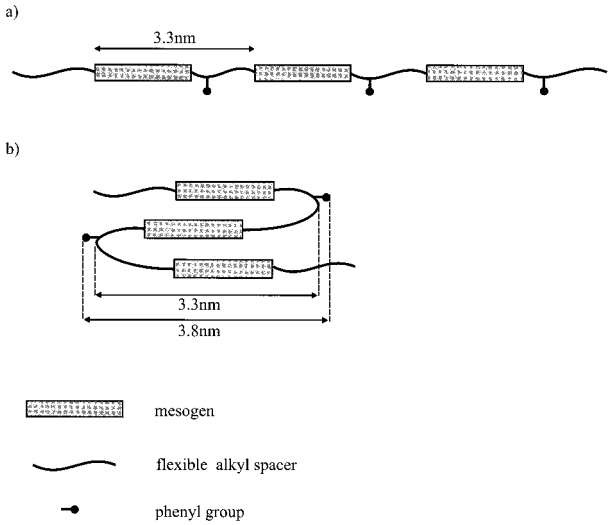

Figure 8. Schematics of the considered chain conformations and the average lengths of the polymer units as estimated by molecular modeling. Model A: chain conformation with a stretched flexible spacer. The length per repeat unit is about 3.3 nm. Model B: chain conformation with a bent flexible spacer to favor regular chain folding ("hairpins"). In contrast to model A, the phenyl group affects the layer spacing. The estimated lengths per repeat unit are about 3.3 nm for P1 and 3.8 nm for P2 and P4.

are compared with the spacings obtained from X-ray data on oriented and unoriented samples of P1, P2, and P4 (Table 2). The data obtained by X-ray diffraction (Table 2) suggest that, at least in oriented fibers of P2 and P4, the chains are folded according to model B. The smaller spacing of about 3.2 nm in the case of P1 does not allow any conclusion about chain folding, since absence of the phenyl group suggests the same spacing for both models. In the case of unoriented samples, the data are not sufficient to distinguish between the two models.

Let us now consider the islands at the surface of the thin films (Figures 5−7), which correspond to exactly one smectic layer. The orientation of smectic layers parallel to the free surface indicates that the mesogens are aligned predominantly perpendicularly to the substrate. Because of the fact that the films are very thin (8, 10, and 7 nm for P1, P2, and P4, respectively) in comparison to the average contour length (67, 38, and 51 nm for P1, P2, and P4, respectively) of the chains, the chains have to fold. This holds for all three samples, P1, P2, and P4. To our surprise, the surface exhibits only two height levels which are attributed to the first (outermost) and second smectic layer. Because of the high polydispersity of the chains, one would expect surface corrugations which correspond to not only one but several smectic layers. Since the surface roughness is dominated by exactly one smectic layer, it can be concluded that the molecules form the typical chain-folded lamellar layers. In these structures each chain is contained in just one layer and folds back on itself many times. Therefore, the observed surface roughness is not induced by the broad polydispersity of (stiff) chains. A relatively smooth surface, which is just modulated by the outermost chain-folded layer of homogeneous thickness, is exposed. This favors obviously model B with the polymer chains regularly folded. In addition, we conclude from the X-ray diffraction a better packing for the polymer with an azobenzene group as the mesogen than for the polymers with an azoxybenzene mesogen. The higher order at lower temperatures, observed for P4 in comparison to P2, may be attributed to a higher ordered smectic phase, like for example a smectic B phase. Annealing at 80 °C may then result in a smectic B → smectic A transition.

In conclusion, we presented the characterization of three main-chain LCPs. All of them organize in smectic mesophases before reaching the isotropic phase at higher temperatures. Of particular interest was the conformation of the chains in the mesophase. A comparison between the length of the repeat units and the smectic layer thickness was not sufficient to distinguish whether the chains are regularly folded or whether they are rather mainly extended. However, on the basis of the structure of ultrathin films (thicknesses of about 2−3 smectic layers), we suggest the model where chains are almost regularly folded.

Acknowledgment. The authors thank Drs. Guido Henn and Britta L. Schürmann for many helpful discussions. This work was partially supported by the European HCM Network under Contract No. CHRX-CT 94 0448.

References and Notes

(1) Watanabe, J.; Hayashi, M.; Nakata, Y.; Niori, T.; Tokita, M. *Prog. Polym. Sci.* **1997**, *22*, 1053.
(2) Zentel, R. In *Liquid Crystals*; Stegemeyer, H., Eds.; Springer: New York, 1994.
(3) de Gennes, P. G. In *Polymer Liquid Crystals*; Cifferry, A., Krigbaum, W. R., Mayer, R. B., Eds.; Academic Press: New York, 1982.
(4) Williams, D. R. M.; Warner, M. *J. Phys. (France)* **1990**, *51*, 317.
(5) Watanabe, J.; Hayashi, M. *Macromolecules* **1988**, *21*, 278.
(6) Watanabe, J.; Hayashi, M. *Macromolecules* **1989**, *22*, 4083.
(7) Tokita, M.; Takahashi, T.; Hayashi, M.; Inomata, K.; Watanabe, J. *Macromolecules* **1996**, *29*, 1345.
(8) Bae, H.; Watanabe, J.; Maeda, Y. *Macromolecules* **1998**, *31*, 5947.
(9) Li, M. H.; Brûlet, A.; Davidson, P.; Keller, P.; Cotton, J. P. *Phys. Rev. Lett.* **1993**, *70*, 2297.
(10) Noirez, L.; Poths, H.; Zentel, R.; Strazielle, C. *Liq. Cryst.* **1995**, *18*, 123.
(11) Reck, B.; Ringsdorf, H. *Makromol. Chem., Rapid Commun.* **1982**, *6*, 291.
(12) Sauvarop, B.; Zentel, R. *Makromol. Chem.* **1988**, *189*, 797.
(13) Wilbert, G.; Zentel, R. *Macromol. Chem. Phys.* **1996**, *197*, 3259.
(14) Wilbert, G.; Traud, S.; Zentel, R. *Macromol. Chem. Phys.* **1997**, *198*, 3769.
(15) Forster, M.; Stamm, M.; Reiter, G.; Hüttenbach, S. *Vacuum* **1990**, *41*, 1441.
(16) Henn, G.; Stamm, M.; Poths, H.; Rücker, M.; Rabe, J. P. *Physica* **1996**, *B221*, 174.
(17) van der Wielen, M. W. J.; Cohen Stuart, M. A.; Fleer, G. J.; de Boer, D. K. G.; Leenaers, A. J. G.; Nieuwhof, R. P.; Marcelis, A. T. M.; Sudhölter, E. J. R. *Langmuir* **1997**, *13*, 4762.
(18) Bernal, J. D.; Crowfoot, D. *Trans. Faraday Soc.* **1933**, *29*, 1032.
(19) Krigbaum, W. R.; Tooru Taga, *Mol. Cryst. Liq. Cryst.* **1973**, *28*, 85.

MA9807567